SAND2010-1717C

HYDROGEN-ASSISTED FRACTURE OF LOW NICKEL CONTENT 304 AND 316L AUSTENITIC STAINLESS STEELS

N.Y.C. Yang,[1] C. San Marchi[1], T.J. Headley[2], J. Michael[2]
[1] *Sandia National Laboratories,7011 East Ave, Livermore CA 94550, USA;*
[2] *Sandia National Laboratories, Albuquerque NM, USA;*
E-mail: *nyyang@sandia.gov*

ABSTRACT

Hydrogen-assisted fracture is observed in austenitic stainless steel alloys. There has been significant debate in the literature about the role of strain-induced martensite on hydrogen-assisted fracture of metastable austenitic stainless steels. It is clear that α'-martensite is not necessary for hydrogen-assisted fracture since hydrogen affects the tensile ductility and fracture properties of stable austenitic stainless steels. Martensite, however, is believed to facilitate hydrogen transport in austenitic stainless steel and numerous studies propose that martensite contributes to fracture. Yet conclusive evidence that strain-induced α'-martensite plays an important mechanistic role on fracture processes in the presence of hydrogen has not been clearly articulated in the literature. In this study, we report microstructural evidence suggesting that α'-martensite does not play a primary role in hydrogen-assisted fracture during tensile testing of metastable austenitic stainless steel. This microstructural evidence also suggests that thermal twin boundaries are susceptible sites for hydrogen-assisted fracture.

KEYWORDS

austenitic stainless steel, hydrogen-assisted fracture, strain-induced martensite, twin boundary fracture

INTRODUCTION

The effects of gaseous hydrogen on the mechanical properties of austenitic stainless steels have been extensively studied [1-6], because austenitic stainless steels are commonly used in high-pressure gaseous hydrogen systems. These studies have focused on nickel content as an important parameter for resistance to hydrogen-assisted fracture; alloys with greater nickel content are generally more resistant to hydrogen-assisted fracture. Nickel strongly influences deformation in austenitic stainless steels, an influence that also appears to be important to the material's resistance to hydrogen-assisted fracture [4]. There is also speculation that strain-induced martensite plays an important role in fracture in the presence of hydrogen [6, 7]; although the role of nickel and martensite are difficult to decouple since greater nickel content generally improves the stability of austenitic stainless steels with respect to formation of strain-induced martensite. There are two primary roles attributed to martensite [6, 7]: (i) enhancement of hydrogen transport into the austenitic matrix; and (ii) nucleation of microstructural damage in the martensite or at the interface between the matrix and the martensite. The goal of this work is to better understand the microstructural features that contribute to hydrogen-assisted fracture in austenitic stainless steels and the effects of hydrogen on deformation and fracture.

alloy	Fe	Cr	Ni	Mo	Mn	Si	C	N	S	P
II	Bal	16.5	10.0	2.0	1.7	0.6	0.022	0.027	0.028	0.029
IV	Bal	18.3	8.6	0.4	1.5	0.4	0.014	0.086	0.029	0.020

Table 1: Composition (wt%) of the alloys examined in this study.

alloy	ASTM grain size	Tensile testing at 293 K			Tensile testing at 223 K		
		Yield strength (MPa)	Reduction of area (%)		Yield strength (MPa)	Reduction of area (%)	
			Non-charged	Hydrogen-precharged		Non-charged	Hydrogen-precharged
II	6	214	82	57	288	78	21
IV	4	221	73	40	312	75	20

Table 2: Microstructural and mechanical properties of the tested materials.

EXPERIMENTAL PROCEDURES

Two austenitic stainless steels were selected from previous studies for extensive microstructural characterization: a 316L alloy (designated as alloy II) and a 304/304L alloy (alloy IV). These alloys were chosen for their relatively low nickel content, being near the minimum generally allowable for 304 and 316 austenitic stainless steels, which are 8 and 10 wt% respectively. The alloys were received in the annealed condition and the composition of these alloys is given in Table 1. The microstructure of these two materials was evaluated before and after deformation using the non-deformed and deformed regions of tensile specimens that were broken at temperature of 223 K; details of the tensile testing are given in Ref. [5] and are consistent with companion studies [3]. In addition, the effect of high concentrations of hydrogen on deformation and fracture were investigated by examining the microstructure and fracture surfaces of tensile specimens that had been tested after thermal precharging with hydrogen. Hydrogen-precharging is intended to simulate the hydrogen content in the material when subjected to stress in a gaseous hydrogen environment. Hydrogen-precharging was conducted by immersion in gaseous hydrogen at pressure of 34.5 MPa and temperature of 300˚C for several weeks. These thermal precharging conditions result in relatively uniform hydrogen content of about 60 wt ppm.

The microstructures were evaluated by optical metallography of polished and etched sections of the materials, as well as scanning electron microscopy (SEM). Broken tensile specimens were also sectioned along the cylindrical axis and prepared for optical metallography; these sections are referred to as longitudinal sections. Electron backscattered diffraction (EBSD) was used to evaluate deformation and damage below the fracture surface on the longitudinal sections. Transmission electron microscopy (TEM) was used to illuminate deformation processes and identify the strain-induced phase transformations by selected-area electron diffraction (SAED). TEM foils were removed from broken tensile specimens just below the fracture surface, in addition to foils of the non-deformed and hydrogen-precharged materials taken from the grip section of the tensile specimens. Fracture surfaces of the broken tensile specimens were also examined by SEM.

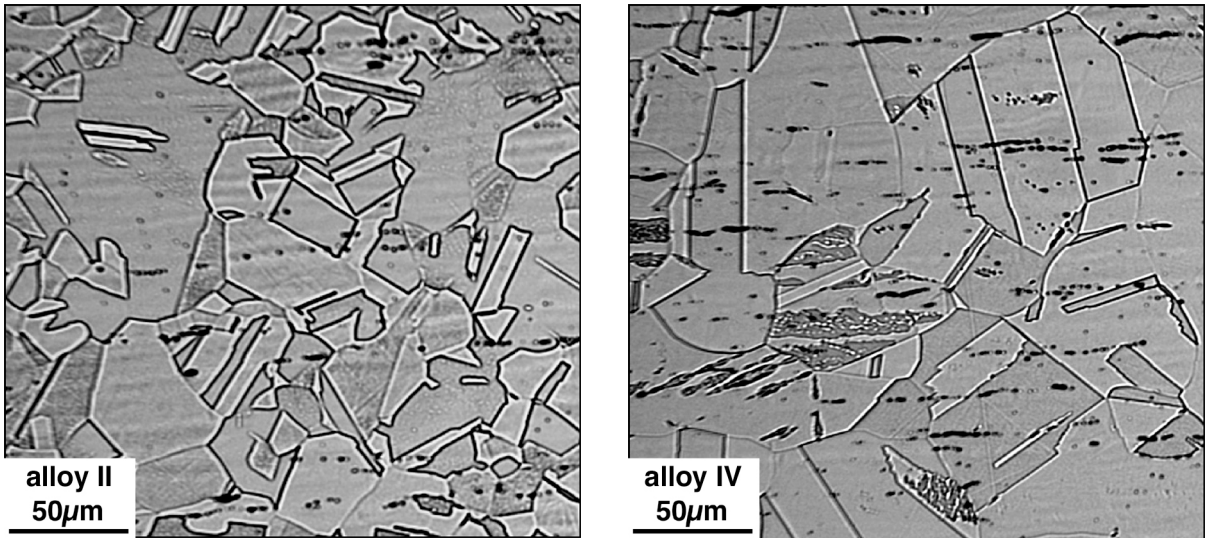

Figure 1: Optical micrographs showing microstructure, including thermal twins.

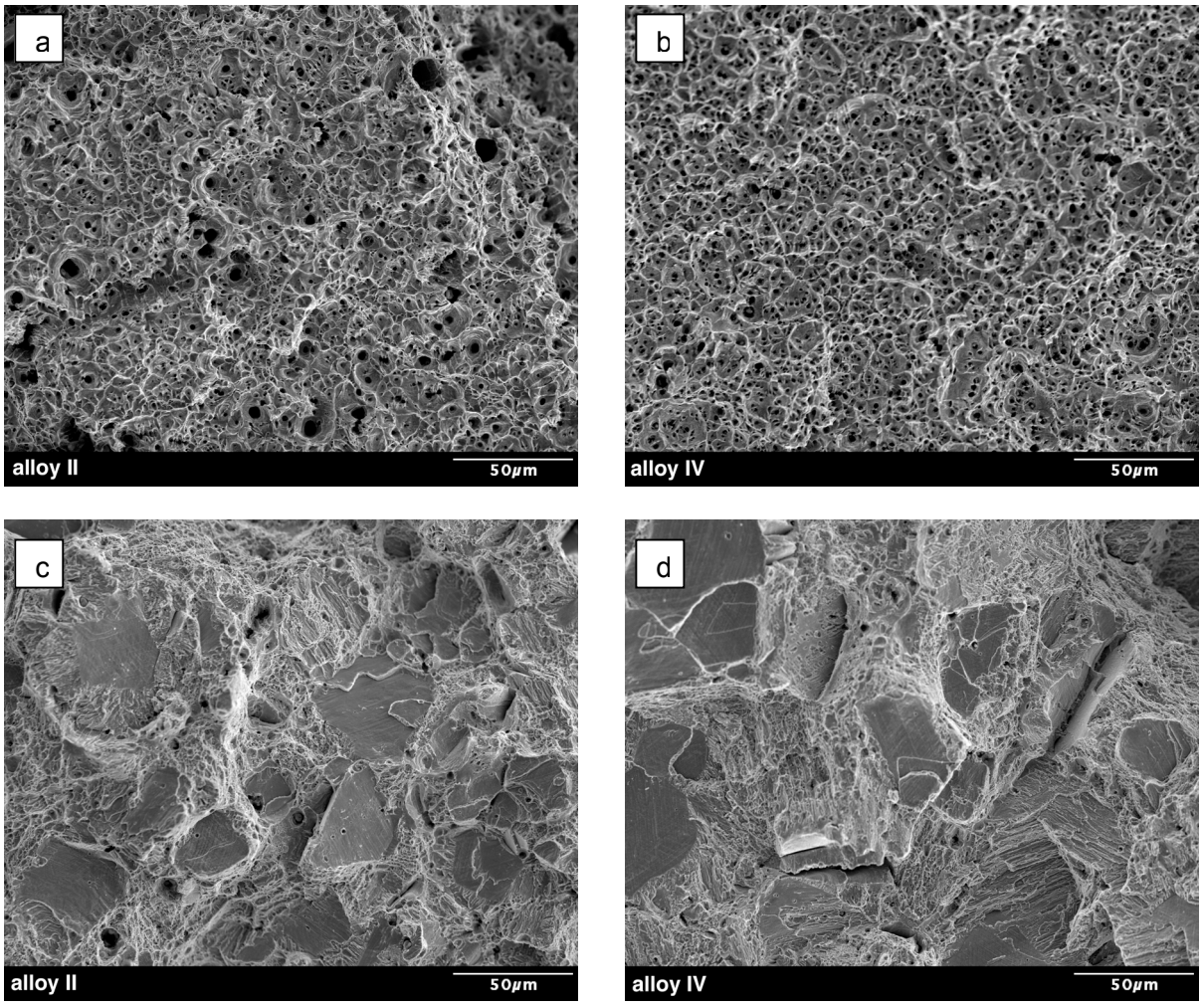

Figure 2: fracture surfaces from tensile specimens tested at 223 K: (a) & (b) non-charged; (c) & (d) hydrogen-precharged.

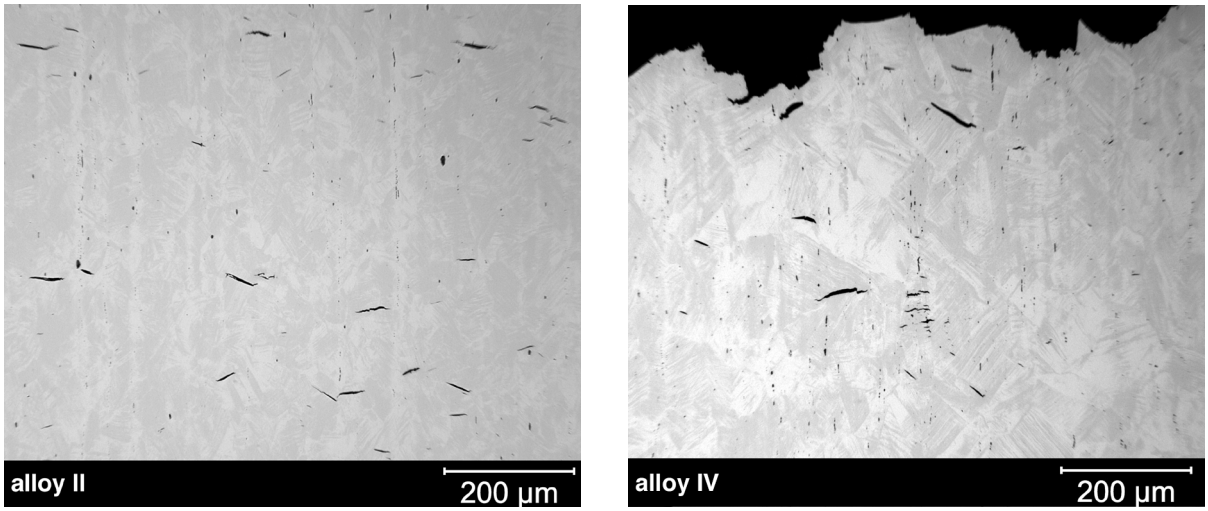

Figure 3: Optical images show the sharp cracks in the gage section (alloy IV shows the profile of fracture surface at the top of the image).

RESULTS AND DISCUSSION

Figure 1 shows typical grain and thermal twin structure of the polished and etched alloys. In general, the grains are equaixed; alloy II has smaller average grain size than alloy IV. In addition, the density of large thermal twins, which often span entire grains, is relatively high for both materials. The yield strength of both alloys is approximately 220 MPa at room temperature and 35 to 40% higher at 223 K (Table 2). The effect of thermally precharging with hydrogen is most apparent in the changes of the material's tensile ductility, as quantified by the reduction of area (RA: percentage decrease in original cross sectional area). The RA is between 70% and 80% in the as-received condition, but drops to as low as 20% when hydrogen-precharged and tested at 223 K (Table 2). Additional tensile data can be found in Refs. [3, 5].

The measured reduction of ductility is also apparent in changes on the fracture surfaces. Fracture surfaces for the alloys in the non-charged and hydrogen-precharged conditions are shown in Figure 2. The non-charged specimens show classic ductile dimples on the fracture surfaces (Figures 2a and 2b), as typical of fracture by microvoid coalescence. With the addition of high concentration of hydrogen, the fracture features are significantly different showing relative flat "facets" surrounded by elongated furrows (Figures 2c and 2d). Polished longitudinal sections of hydrogen-precharged tensile specimens (Figure 3) reveal sharp, relatively straight cracks below the fracture surface, which are nominally perpendicular to the loading axis. These subsurface cracks are nominally the same size as the facets on the fracture surface, suggesting that this damage is consistent with the "facets" on the fracture surface. Moreover, these cracks are distributed throughout the gauge length (but absent from the non-deformed regions), implying that they begin to develop relatively early in the strain history.

Flat "facets" have been previously observed in fracture surfaces of austenitic stainless steels and these were interpreted to be fracture of twin boundaries [8, 9]. On the other hand, strain-induced martensite is often invoked as an explanation for fracture mode changes in austenitic stainless steel exposed to hydrogen, although the microstructural evidence for this latter interpretation is absent and considered neither a necessary nor sufficient condition for hydrogen-assisted fracture [10]. In an effort to identify microstructural features that may be associated the large facets, areas around the subsurface cracks in longitudinal sections of alloy IV were investigated using EBSD (Figure 4). In a few cases, cracks could not be

associated with microstructure by EBSD, these cracks tended to be less straight than most of the subsurface cracks. The majority of analyzed cracks, however, showed that fracture occurred along twin boundaries. Inverse pole figures show that the grains on either side of the crack are rotated by 60 degrees with respect to one another (Figure 4d), indicative of a twin relationship. In addition, the crack stops at precisely the location where the twin relationship is lost. Strain-induced α'-martensite was clearly resolved as well, but the martensite boundaries were not coincident with the fracture facet.

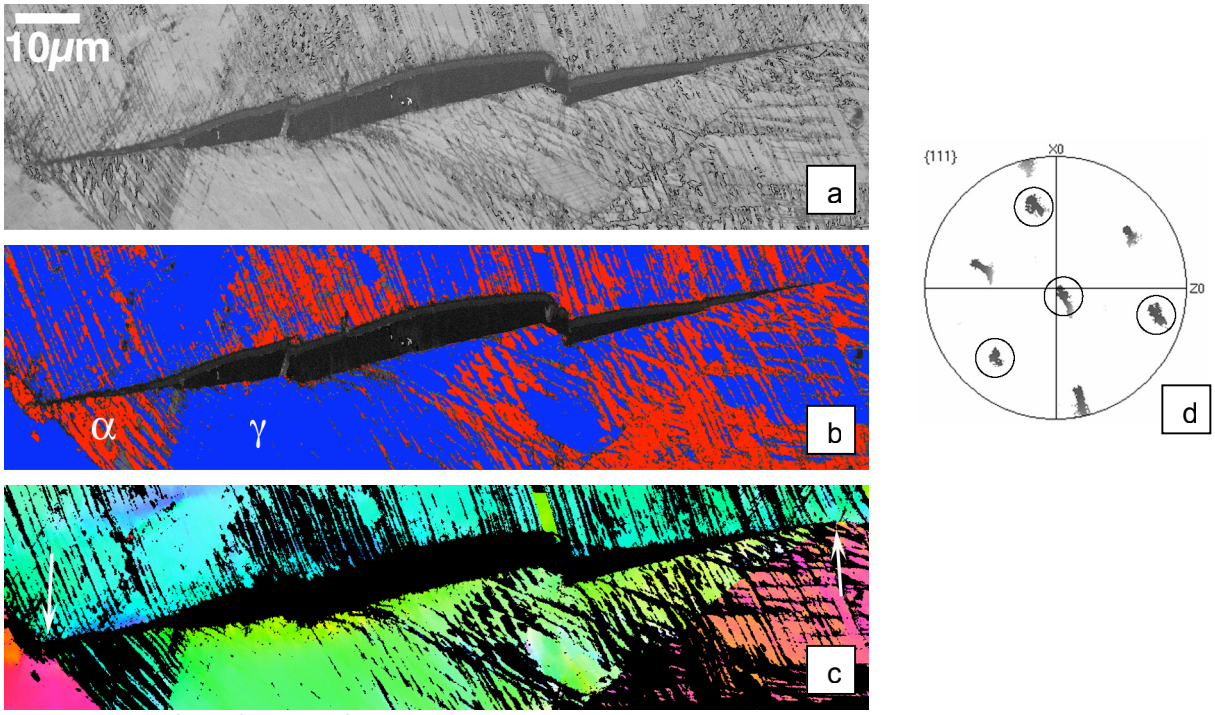

Figure 4: EBSD of subsurface crack in alloy IV: (a) backscattered electron image; (b) phase map shows γ-austenite in blue (FCC) and α'-martensite in red (BCC); (c) inverse pole figure map shows crack terminates when orientation relationship across boundary changes (arrows); and (d) inverse pole figure shows 60˚ rotation between upper (circled) and lower grains, indicative of a twin boundary.

TEM shows that both ε-maternsite and α'-martensite are present in the specimens deformed at 223 K (Figures 5 and 6). There is no evidence of martensite (or other microstructural changes) in hydrogen-precharged material that had not been deformed (Figures 5a and 6a). The martensitic transformations in 304 stainless steel have been identified as γ→ε→α' [11], although it is reported that ε-martensite is not a requisite for the nucleation of α'-martensite [12]. In this study, α'-martensite with the Nishiyama-Wassermann orientation relationship was found to nucleate at the intersection of ε-martensite platelets (the latter having the Shoji-Nishiyama orientation relationship with the austenite matrix). Larger platelets of α'-martensite tend to have the Kurdgumov-Sachs orientation with the austenite (also reported elsewhere [11]) and are interleaved with parallel ε-martensite platelets. The results in a fixed relationship between contiguous ε-martensite and α'-martensite in these layered regions.

In alloy II (the higher nickel containing alloy), mechanical twinning was apparent in SAED patterns, but no evidence of mechanical twinning was apparent in alloy IV. Although difficult to quantify, it was additionally noted that less ε-martensite is present in alloy II compared to alloy IV. Mechanical twins and ε-martensite are related by the structure of overlapping stacking faults [13]: if stacking faults overlap on adjacent {111} planes, a mechanical twin

(sometimes called a deformation twin) is formed, while ε-martensite is formed by overlap on every other {111} plane. These results, combined with the observation that austenitic stainless steels tend to deformation by twinning at high stress [14], then suggest that hydrogen may have a tendency to promote the formation of ε-martensite at the expense of mechanical twinning. More work is necessary to clarify the effects of hydrogen on deformation and transformation, in part because mechanical twinning and formation of ε-martensite also depend on nickel content and temperature [12].

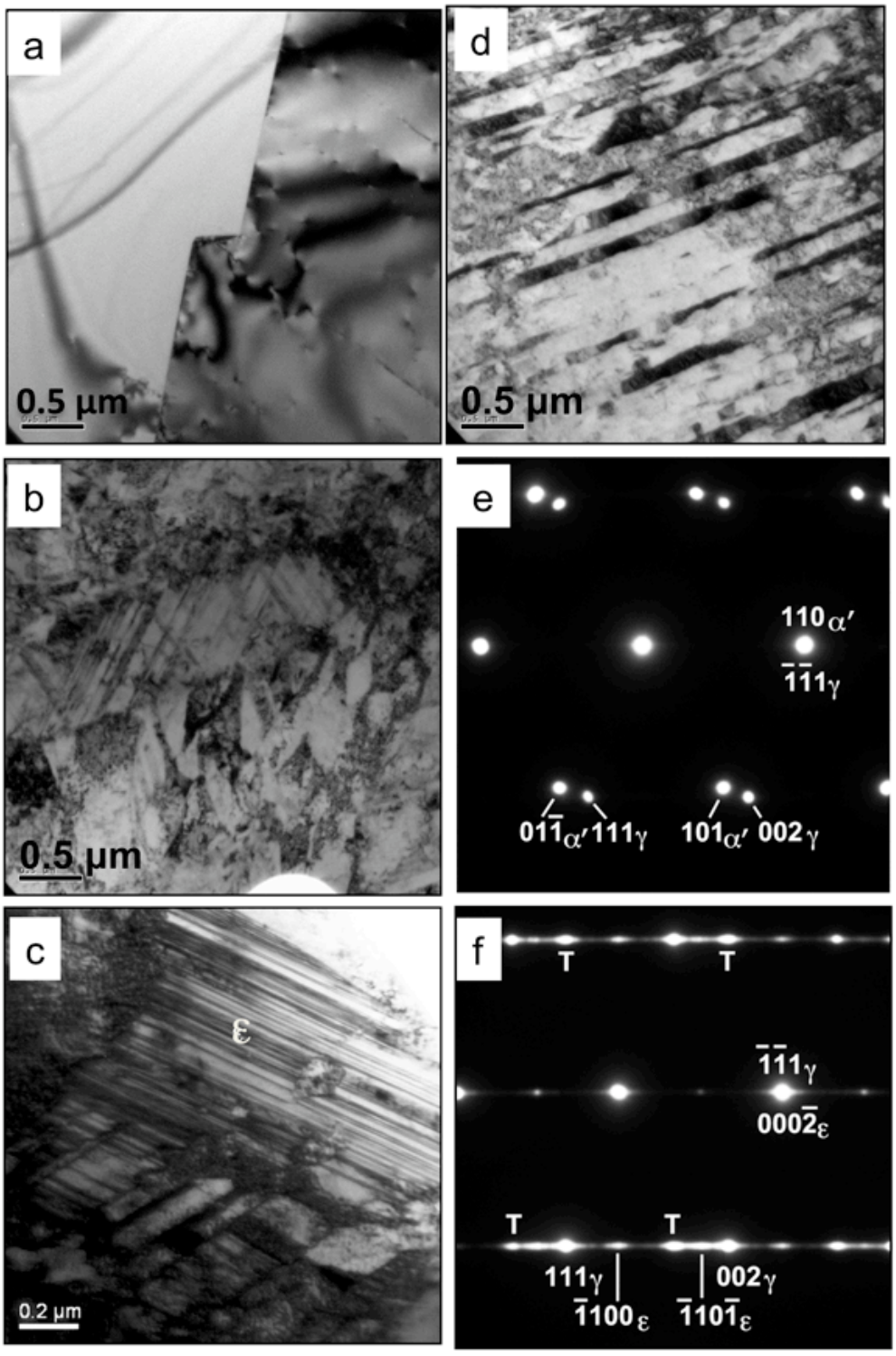

Figure 5: TEM-bright field (BF) images and SAED of alloy II: (a) non-deformed grip section; (b) strain-induced α'-martensite and ε-martensite; (c) dense thin platelets of ε-martensite; (d) dense α'-martensite platelets; (e) SAED identifying α'-martensite; (f) SAED identifying ε-martensite and mechanical twinning (T).

SUMMARY AND CONCLUSIONS

Hydrogen-assisted fracture can significantly reduce the tensile ductility of austenitic stainless steels. Relatively flat "facets" are observed on the fracture surface of alloys with relatively low nickel content that have been thermally precharged with hydrogen and tested at temperature of 223 K. Microstructural characterization using EBSD shows that these facets are consistent with thermal twin boundaries. Strain-induced martensite does not appear to play a direct role in the formation of these facets; however, TEM images confirm that both ε-martensite and α'-martensite are formed during deformation. Given the close relationship between strain-induced ε-martensite and mechanical twinning, these results also suggest that hydrogen may promote the formation of ε-martensite.

ACKNOWLEGEMENTS

The authors would like to acknowledge Ken Lee and Roger Watson for their assistance with testing at Sandia National Laboratories, and Jeff Campbell for performing the hydrogen precharging, also at Sandia. Sandia is a multiprogram laboratory operated by Sandia Corporation, a Lockheed Martin Company, for the United States Department of Energy under contract DE-AC04-94AL85000.

REFERENCES

1. G.R. Caskey, Hydrogen Effects in Stainless Steels, in: Oriani RA, Hirth JP and Smialowski M, editors, Hydrogen Degradation of Ferrous Alloys, Noyes Publications, Park Ridge NJ, 1985, pp. 822-862.
2. C. San Marchi, B.P. Somerday, X. Tang and G.H. Schiroky, Hydrogen-assisted fracture of type 316 stainless steel at subambient temperature (PVP2008-61240), in: Proceedings of PVP-2008: ASME Pressure Vessels and Piping Division Conference (Chicago IL, 2008), ASME,
3. T. Michler, A.A. Yukhimchuk and J. Naumann, Hydrogen environment embrittlement testing at low temperatures and high pressures, Corros Sci 60 (2008) 3519-3526.
4. C. San Marchi, K.A. Nibur, D.K. Balch, B.P. Somerday, X. Tang, G.H. Schiroky and T. Michler, Hydrogen-assisted fracture of austenitic stainless steels, in: Somerday BP, Sofronis P and Jones R, editors, Effects of Hydrogen on Materials, Proceedings of the 2008 International Hydrogen Conference (Moran WY, 2008), ASM International, Materials Park OH, 2009, pp. 88-96.
5. C. San Marchi, T. Michler, K.A. Nibur and B.P. Somerday, Tensile testing of type 304 and 316 austenitic stainless steels with internal and external hydrogen, Int J Hydrogen Energy (accepted) (2010)
6. L. Zhang, M. Wen, M. Imade, S. Fukuyama and K. Yokogawa, Effect of nickel equivalent on hydrogen gas embrittlement of austenitic stainless steels based on type 316 at low temperatures, Acta Mater 56 (2008) 3414-3421.

7. Y. Mine, C. Narazaki, K. Murakami, S. Matsuoka and Y. Murakami, Hydrogen transport in solution-treated and pre-strained austenitic stainless steels and its role in hydrogen-enhanced fatigue crack growth, Int J Hydrogen Energy 34 (2009) 1097-1107.
8. G.R. Caskey, Fractography of hydrogen-embrittled stainless steel, Scr Metall 11 (1977) 1077-1083.
9. G.R. Caskey, Hydrogen-induced brittle fracture of type 304L austenitic stainless steel, in: Gilbertson LN and Zipp RD, editors, Fractography and Materials Science, ASTM STP733, American Society of Testing and Materials, Philadelphia PA, 1981, pp. 86-77.
10. G.R. Caskey, The role of twinning and transformation in hydrogen embrittlement of austenitic stainless steels, in: Louthan MR and McNitt RP, editors, Environmental Degradation of Engineering Materials, Virginia Polytechnic Institute, Blackburg VA, 1977, pp. 437-449.
11. P.L. Mangonon and G. Thomas, The martensite phases in 304 stainless steel, Metall Trans 1 (1970) 1577-1586.
12. F. Lecroisey and A. Pineau, Martensitic transformation induced by plastic deformation in the Fe-Ni-Cr-C system, Metall Trans 3 (1972) 387-396.
13. J. Talonen and H. Hanninen, Formation of shear bands and strain-induced martensite during plastic deformation of metastable austenitic stainless steels, Acta Mater 55 (2007) 6108-6118.
14. T.S. Byun, N. Hashimoto and K. Farrell, Deformation mode map of irradiated 316 stainless steel in true stress-dose space, J Nucl Mater 351 (2006) 303-315.

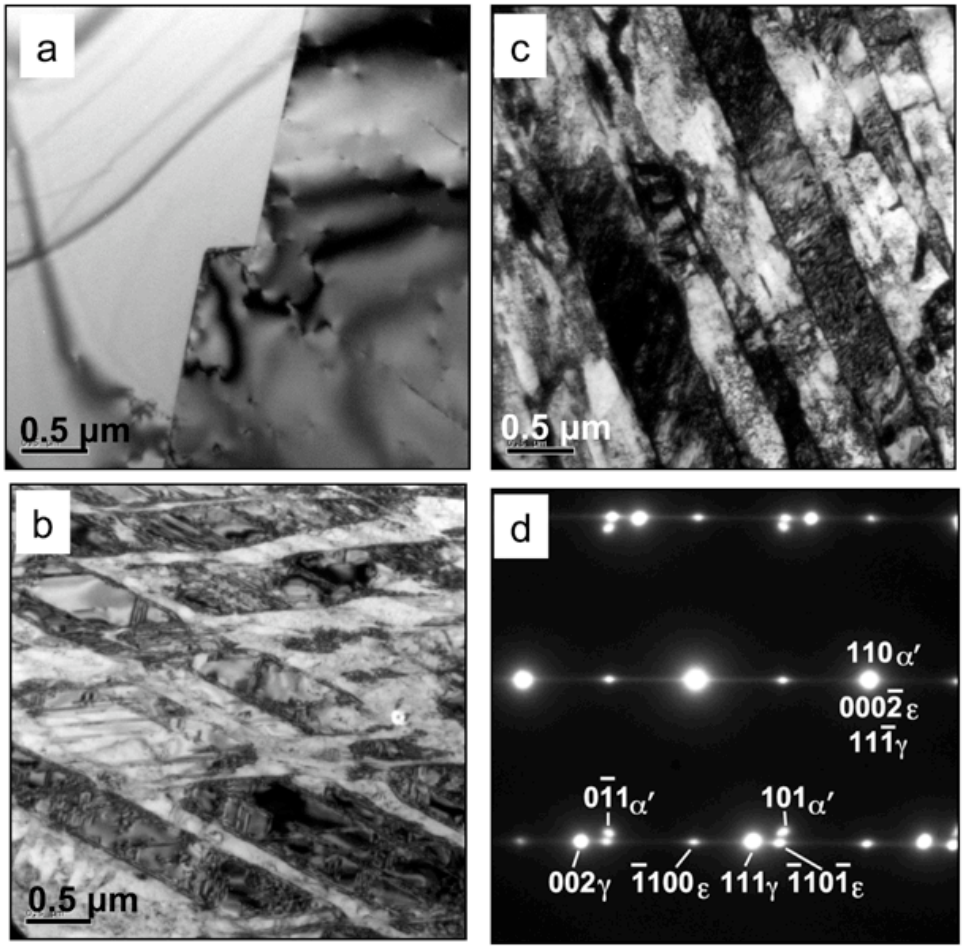

Figure 6: TEM-bright field (BF) images and SAED of alloy IV: (a) non-deformed grip section; (b) α'-martensite with thin ε-martensite platelets; (c) large bands of α'-martensite; (d) SAED identifying α'-martensite and ε-martensite. Deformation twinning was not observed in alloy II.